Optical fiber-based sensors for real-time monitoring for low-energy proton beams

Fiammetta Fricano, Luca Weninger, Adriana Morana, Amor Romero Maestre, Pedro Martín-Holgado, Jose de Martin Hernandez, Yolanda Morilla, Damien Lambert, Philippe Paillet, Hicham El Hamzaoui, et al.

Optical Fiber-based Sensors for Real-Time Monitoring for Low-Energy Proton Beams

Fiammetta Fricano, Luca Weninger, Adriana Morana, Amor Romero Maestre, Pedro Martín-Holgado, Jose De Martin Hernandez, Yolanda Morilla, Damien Lambert, Philippe Paillet, Hicham El Hamzaoui, Bruno Capoen, Mohamed Bouazaoui, Emmanuel Marin, Youcef Ouerdane, Aziz Boukenter, Sylvain Girard*

*corresponding author

F. Fricano, L. Weninger, A. Morana, E. Marin, Y. Ouerdane, A. Boukenter, S. Girard
Hubert Curien Laboratory, Jean Monnet University, Saint Etienne, France
E-mail: fiammetta.fricano@univ-st-etienne.fr

A. Romero Maestre, P. Martín-Holgado, J. De Martin Hernandez, Y. Morilla
Centro Nacional de Aceleradores, Universidad de Sevilla-CSIC-JA, Sevilla, Spain

F. Fricano, D. Lambert, P. Paillet
CEA/CESTA, CS60001, 15 Avenue des Salinières, 33116 Le Barp, France

H. El Hamzaoui, B. Capoen, M. Bouazaoui
Univ. Lille, CNRS, UMR 8523 - Physique des Lasers Atomes et Molécules (PhLAM), F-59000, Lille, France

S. Girard
Institut Universitaire de France (IUF), Paris, France

Funding: The results presented in this paper have been obtained in the framework of the EU project RADNEXT, receiving funding from the European Union's Horizon 2020 research and innovation program, Grant Agreement no. 101008126

Keywords: optical fibers, radioluminescence, protons, dosimetry

Abstract: This work presents the first results from our investigation regarding the potential use of radioluminescent Ce^{3+}-doped silica-based optical fibers as sensors capable of monitoring the flux of low-energy (≤ 15 MeV) protons. This technology is shown as a promising candidate for

dosimetry at the Centro Nacional de Aceleradores (CNA), offering improved precision and real-time radiation monitoring during radiation test campaigns on microelectronics or photonics components and devices. Two proton beam lines have been used to characterize the fiber dosimeters in two different CNA facilities, using a 18/9 Cyclotron and a Tandem 3 MV accelerators. The calibration of the sensor for monitoring the proton flux at 15 MeV is currently reliable within a 24% margin, due to the presence of significant beam fluctuations that prevent a unique correlation between radioluminescence levels and the associated flux values. However, this result can be improved through additional tests aimed at refining the calibration process. When using 3 MeV protons, the signal exhibits an enhanced radioluminescence, confirming the high sensitivity of optical fibers to low-energy protons. Physically relevant insights are obtained, as the compact geometry of the optical fiber makes it sufficiently embedded to detect the 3 MeV proton Bragg peak within its sensitive core region. Nevertheless, further investigations are needed to fully understand the radioluminescence mechanism, especially under the high dose rate conditions involved.

1. Introduction

Ionizing radiation refers to radiation capable of breaking chemical bonds and potentially altering the physical and chemical properties of the interacting material. Among ionizing radiations, protons are present in various harsh environments and they can affect both living tissue and electronic components, making it essential to monitor them and mitigate their effects. For example, radiation environments such as space are rich of protons with energies in the MeV range.[1] Especially in Medium Earth orbit (MEO) and Geostationary Earth orbit (GEO), we can find protons having low energy, between a few MeV and 10 MeV. These protons must be carefully monitored to ensure the safety of both human life and the electronic equipment used in space missions.[2] Moreover, protons are extensively used in medical applications, especially in proton therapy treatments. This technique takes advantage of the fact that protons deposit the majority of their energy at a specific depth within tissue, known as the Bragg peak.[3] This allows for the precise targeting of tumor regions while minimizing damage to the surrounding healthy tissues.

Due to these reasons, among the main challenges in dosimetry research is the ability to measure in real-time and precisely proton particle flux. One of the most promising technologies for this purpose is optical fiber technology, which offer numerous advantages, including ease of use, simple setup, and straightforward calibration procedures.[4,5] By exploiting radiation-induced effects in optical fibers, such as Radiation Induced Attenuation (RIA) and Radiation Induced Luminescence (RIL or RL), it is possible to monitor ionizing particles fluxes and fluences.[6] RIL phenomenon, exploited for this study, consists in spontaneous light emission caused by the recombination of released electrons due to radiation. These electrons can either become trapped in deep traps (explaining effects such as the Bright Burn Effect (BBE))[7] or recombine at luminescent centers, emitting mainly visible light that can be easily detected with state-of-the-art detectors. This collected light signal is ideally linearly proportional to the dose rate (flux), enabling real-time monitoring of dosimetric quantities.[8] This approach can be applied to all types of ionizing radiation, yielding similar results since the Total Ionizing Dose (TID) remains the main factor responsible for radiation-induced changes in silica-based optical fibers.

The RIL phenomenon can be enhanced by the presence of specific dopants incorporated in the silica matrix.[6,9] Among the various radioluminescent dopants, trivalent cerium ion (Ce^{3+}) is often used due to its relatively intense luminescence at 480 nm.[10,11] and the good linear response of its RIL with respect to the dose rate.[12] Promising results by using a Ce^{3+}-doped optical fiber have already been reported for both 20 to 74 MeV proton and 14 MeV neutron monitoring in various facilities, respectively TRIUMF in Canada [13, 14] and ENEA in Italy [15],

but also for electrons [16] and X-rays.[17] Pre-treatment strategies, such as pre-irradiating the fibers, can be employed since they demonstrated several benefits, including enhanced radiation sensitivity.[18,19] This justifies a direct comparison between pristine (i.e. never irradiated fiber) and irradiated samples, to highlight the effects of cumulative ionizing dose and to provide insight into their long-term performance for extended operational use. In this study, Ce^{3+}-doped optical fiber is proposed as an advanced dosimetric system for the Centro Nacional de Aceleradores (CNA) facility, where protons with low energies (≤ 15 MeV) can be produced. The research center is engaged for several research activities, spacing from materials science, biomedicine and environmental science.[20] For this study, a first facility, based on a 18/9 cyclotron, is used to obtain protons at 15 MeV. Additionally, 3 MV Tandem accelerator is employed to obtain protons in the 2 to 5 MeV range. Physically relevant results are obtained at lower energies, since the Bragg peak of the protons occurs within the fiber core (i. e. the sensitive part of the dosimeter).

2. Materials and Methods

2.1. Optical fibers

The tested samples are silica-based optical fibers in which cerium ions were incorporated using the sol-gel technique[12], performed by the PhLAM Laboratory of Lille (France). The fiber presents a ~121 μm diameter pure silica core, whose 52 μm inner diameter was doped with 0.07 wt% of Ce. They are coated with a first low refractive index material (209 μm diameter), primarily composed of 1-Propanone, 2-hydroxy-2-methyl-1-phenyl, to ensure the light guidance in the silica core, and with a second polymer coating (288 μm diameter), to enhance their mechanical strength. The samples, in any case, were uncoated in order to perform the splice with the transport fiber. Specifically, we tested one pristine sample (never exposed to radiation) and one pre-irradiated sample, which had been exposed to X-rays up to a TID of 500 kGy(SiO_2). This pre-irradiated fiber was pre-calibrated under X-rays at the Hubert Curien Laboratory (Saint-Étienne, France), by monitoring the RIL levels during short irradiations (20 seconds) at different dose rates. This allowed the estimation of a sensitivity coefficient, equal to 1747 counts/mGy, which can then be used to estimate the dose rates once the fiber is tested at the CNA facility.

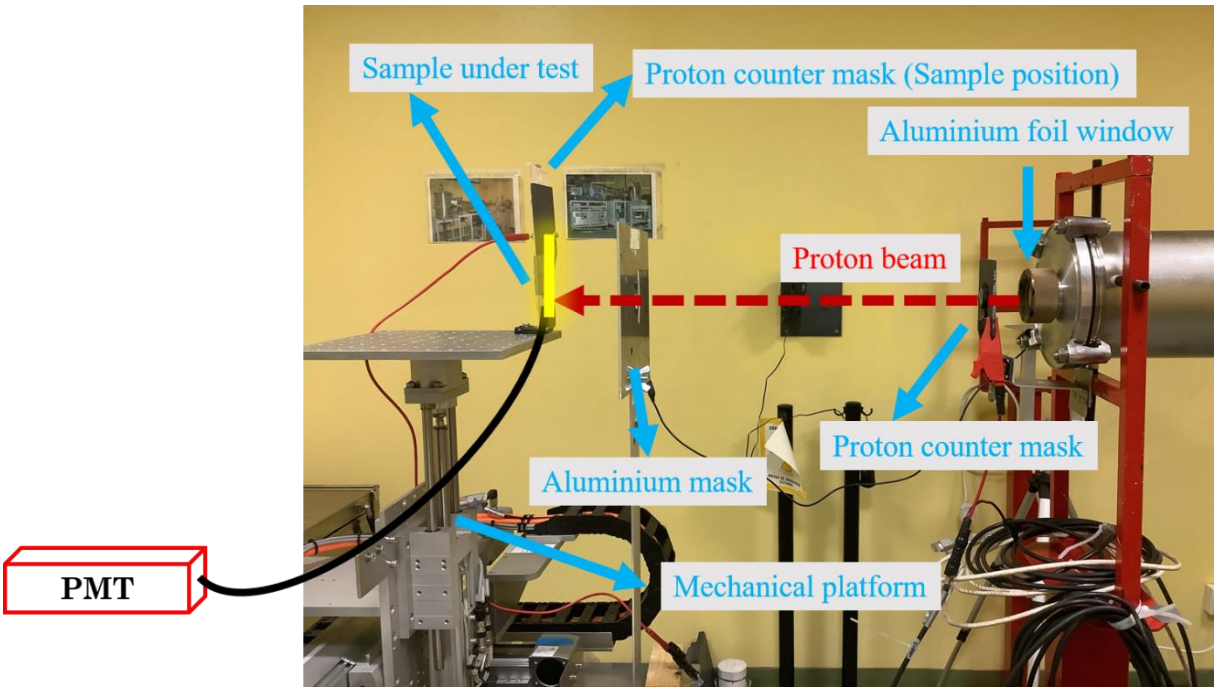

Figure 1: Schematic setup in the CNA cyclotron external beam line.

2.2 Proton beam facilities

The measurements were carried in the Centro Nacional de Aceleradores (CNA) (Sevilla, Spain). The protons are produced by 18/9 cyclotron machine, usually employed for radioisotopes production or for the research beam line. [21] It delivers protons at 18 MeV inside the irradiation line but, in this case, we worked in air, using the external irradiation line. Due to this, the energy was lowered to 15 MeV, with estimated spread in the order of 400 keV. This energy of the incident beam is obtained using the energy loss data calculated with the SRIM2013 code.[22] **Figure 1** gives the general scheme of our selected experimental configuration. The proton beam exits from an aluminum foil window (thickness of 100 µm). Then, it passes through a graphite proton counter mask that acts as beam collimator and proton flux monitor. During the runs, the flux is monitored by the facility staff indirectly through the integration of the beam current though such mask, by using a Brookhaven 1000c current integrator. The current extracted from the cyclotron depends on the current supplied to the source. Currents of nA and pA were used in this work. An aluminum mask with 2 cm diameter hole is then used to have more than 90% beam uniformity in a circular area with a diameter of 2 cm. The beam finally reaches the samples under test and another graphite proton counter mask. In this work, they were both placed at 53 cm from the exit nozzle and on a remotely controlled mechanical platform. This second proton counter mask is used to double check the current (flux) that will arrive at the sample position. During irradiation, it is in fact not possible to measure the flux that arrives to

the samples. The calibration is done by comparing the measured current from both counter masks.

The lower energy protons (3-5 MeV) were instead produced in the 3 MV Tandem pelletron accelerator, able to provide energies between 600 keV and 6 MeV. This facility is also dedicated to material characterization and the development of nuclear instrumentation, particularly radiation detectors.[21] The irradiation beam line, located downstream of the accelerator, was equipped with several devices for beam focusing, steering, and monitoring. At the end of the line, the vacuum chamber with the corresponding electrically insulated sample-holder was placed. The setup configuration scheme for the Tandem facility is very similar to the one presented in **Figure 1** but working in vacuum ($P \sim 10^{-6}$ mbar). For this reason, the use of a fibered vacuum feedthrough was needed to ensure that the radioluminescence could be monitored from outside the vacuum chamber. In the range of the used fluxes, from $\sim 10^{8}$ particles cm^{-2} s^{-1}, the beam intensity was measured directly on the sample holder, which was biased at 200-300 V to collect the secondary electrons and connected to a Brookhaven 1000c current integrator. For both facilities, the total fluence is calculated based on the value of the particle density over the entire irradiated area, multiplied by the run duration. The uncertainty associated with flux and fluence measurements is within 10 %. Depending on the runs, the pulses were acquired using 0.1nA over 6 nA or 0.5 nA over 20 nA sensitivity scales.

2.3 RIL setup

The 2 cm-long samples were placed on the previously mentioned sample holder and aligned with the collimator-beam axis through mechanical adjustments of the remote-controlled platforms. Within the same irradiation spot, it was possible to place two fibers in parallel, allowing for a simultaneous study of their responses. In the case of the tandem, we fixed the fibers on a sample holder designed for the vacuum chamber. An extra support allowed samples to be electrically isolated, since the flux is calculated by collecting the charge on the sample holder. Also, the sample holder in the tandem is movable (x-y) using external controls. In both facilities, the pigtails spliced to each probe were connected to dedicated signal transmission cables, optimized for signal transport along the bunker of the irradiation rooms to the acquisition system. The latter consisted of two photomultiplier tubes (PMTs) capable of collecting photons in the visible range. Using two identical detectors, we simultaneously monitored pristine and pre-irradiated fibers under the same conditions, following the RIL kinetics with a gate time of 200 ms. The transport system consisted in pure-silica-core optical fibers covered by a specific black tube to reduce ambient light contribution. An attenuator was placed in the acquisition chain for highest fluxes, to avoid reaching the saturation level of the

PMTs. This was taken into account during the analysis.

It is worth noting that no Cherenkov effect was expected during these measurements since the kinetic energy required to observe this light emission in air or vacuum is significantly above 15 MeV.[23,24] This confirms that all detected optical emissions originated from intrinsic radioluminescence processes within the fiber material.

2.4 Monte Carlo simulations

We used Geant4 10.7.4 simulation tool [25, 26] to model the tested fiber geometry and to determine the dose deposited within the fiber doped core, i. e. the sensitive volume. Fiber geometry modeling considered the various layers (doped core, core and coatings) and their associated materials (respectively Ce^{3+}-doped silica, pure-silica, acrylate). Fibers were modelled as multilayered cylinders and the silica density was assumed to be 2.2 g/cm^3. As for the experiments, proton trajectories are perpendicular to the fiber propagation axis. The used library is the QGSP_BERT_EMZ which is compliant with the incident particle species and energies and with the scale of the fibers. A large number of primaries (~10^7) were launch multiple times in order to have a good statistic (below 1% of uncertainty) and accurate simulation results.

3. Results and Discussion

3.1. 15 MeV protons

Figure 2 shows an example of the RIL measured for the two optical fibers (pristine and pre-irradiated) for four irradiation runs characterized by different 15 MeV proton fluxes. These were not selected in a specific order other than to test the flux monitoring capability at a fixed energy of 15 MeV. As expected, the RIL levels from the pre-irradiated fiber are higher than the pristine ones (within a 13%, considering all the error sources from the two distinguished setup acquisition chains), confirming enhanced radioluminescence signal by pre-irradiation. During individual runs, the signal was not constant but exhibited several small fluctuations that are associated with the facility operation. The normalized by the respective maximum signals in **Figure 3(a)** reveal no significant difference between the responses of the two independent measurement channels; parallel monitoring indeed allows us to distinguish between variations due to changes in the facility beam flux, which affected both samples equally, and those caused by the different histories of the two fibers. Moreover, plotting the data of one channel as a function of the other, simultaneously acquired, allows estimating the agreement between the

two independent data sets. As shown in **Figure 3(b)**, we observe a good correlation between the two channels, confirming that same beam fluctuations have been recorded.

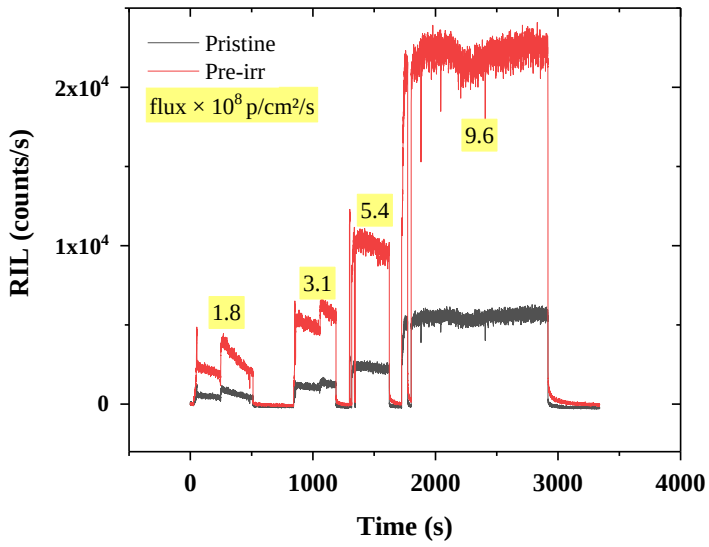

Figure 2: RIL kinetics of pristine and pre-irradiated Ce^{3+}-doped samples during irradiation runs at different 15 MeV proton fluxes.

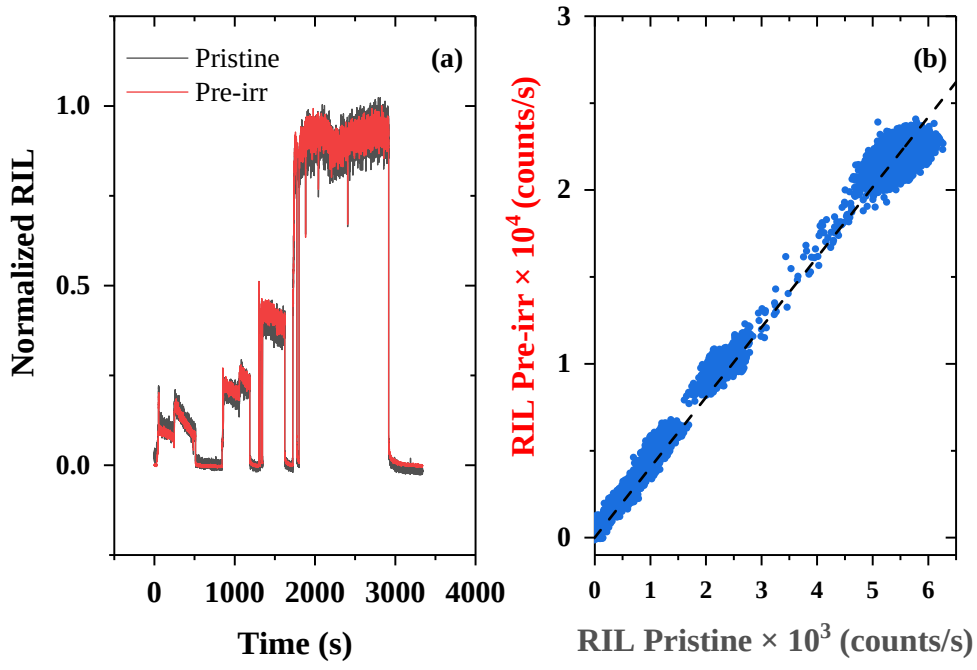

Figure 3: (a) Normalized RIL kinetics. (b) Two channels correlation.

In **Figure 4(a-b)** the RIL levels measured during all the runs of the irradiation campaign are correlated, respectively, with the proton flux values provided by the facility and with the proton fluence, calculated as multiplication of the nominal proton flux, given by the facility, by the irradiation time for each run. More data points are presented for the pre-irradiated fiber because

this sample was also used as a reference in additional runs involving comparisons with differently doped optical fibers (not discussed here), whereas the pristine fiber was tested in parallel only with its pre-irradiated counterpart. The errors associated with the RIL and the integrated RIL (iRIL) come from the sum of the standard deviations of the mean RIL level value and the mean noise acquired before each run. The x-error bars are the 10% of the flux (or fluence) value, as estimated by the facility. The response appears linear for both fibers, allowing a linear fit to be performed and thus enabling the calibration of the fiber.

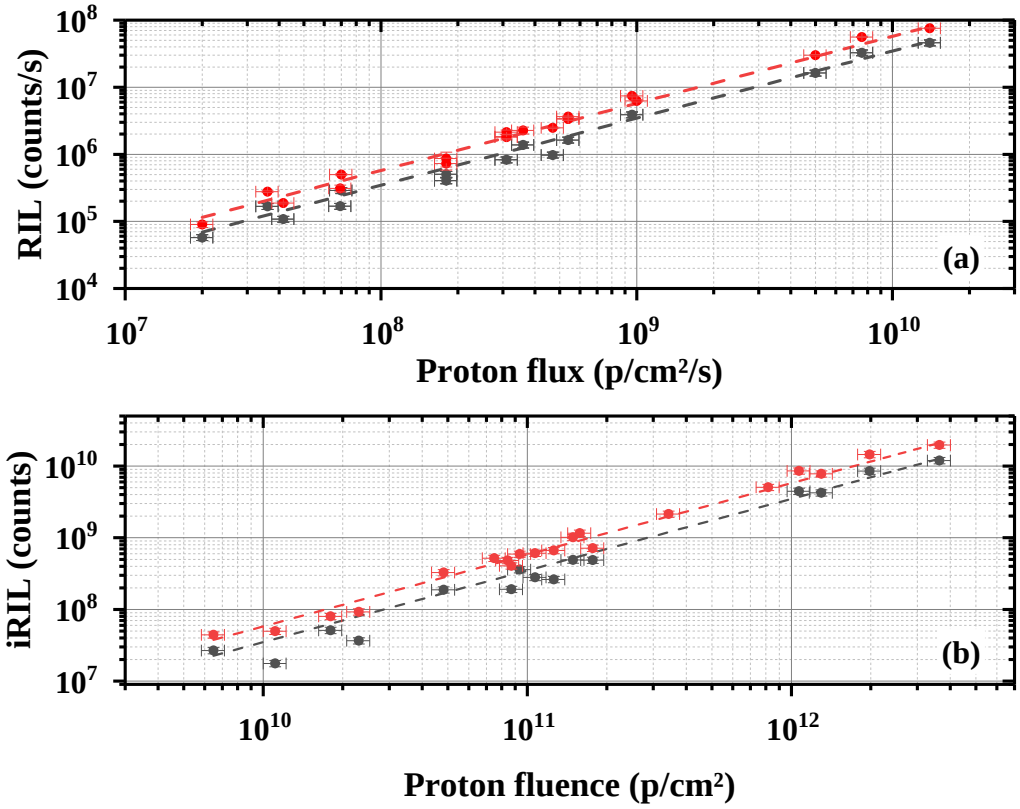

Figure 4: (a) RIL levels vs nominal proton flux values, provided by the facility; (b) Integrated RIL vs proton fluence. The red dots are the data from the pre-irradiated fiber, whereas the black ones are for the pristine sample. Dashed lines represent the linear fits. Y-error bars are often smaller than the data point size.

From the linear fits, we obtained the sensitivities reported in **Table 1**. The sensitivity to flux or fluence, in fact, physically represents the calibration factor of the proposed dosimeter. It is noteworthy that the pre-irradiated fiber has almost twice higher sensitivity than the pristine one, clearly demonstrating the enhancement induced by the pre-irradiation treatment. In principle, the sensitivities obtained vs the two different quantities (flux and fluence) are consistent, within

approximately 3%, since only a multiplicative constant (the irradiation time) is involved in their determination.

Moreover, the data dispersion with respect to the fluence is increased, as observed by the R^2 value, probably because the nominal fluence is deduced by simple multiplication of the proton flux by the irradiation run time. However, the radioluminescence kinetics (as recorded through the multi-channel acquisition system), as shown in **Figure 2**, reveal that the beam is not stable and exhibits significant fluctuations, which are not currently monitored by the facility. This undoubtedly affects the reliability of the calibration performed at the irradiation facility, but demonstrates the potential of optical fibers as an accurate system to monitor the beam evolution.

Table 1. Sensitivities for the pristine and the pre-irradiated fibers, obtained as a function of the nominal proton flux and proton fluence.

Optical fiber	(vs Flux) Sensitivity (counts/p/cm²)	R^2	(vs Fluence) Sensitivity (counts/p/cm²)	R^2
Pristine	3.54×10^{-3}	0.99376	3.64×10^{-3}	0.95829
Pre-irradiated	5.83×10^{-3}	0.99941	5.06×10^{-3}	0.98558

A first estimation of the calibration reliability can be obtained from Geant4 simulations. **Figure 5** shows the absorbed dose per unit of proton fluence as a function of proton energy, calculated for a geometry that approximates the cerium-doped optical fiber, as described in Section 2.3. The curve corresponding to the cerium-doped core (red dots) is compared with SRIM [21] data for a silica bulk sample (solid line). When the two curves overlap, electronic equilibrium is achieved, and the geometry does not influence the dose deposition.

This condition is not fulfilled at lower energies, as the Bragg peak occurs within the fiber core due to the reduced penetration power of low-energy protons. This aspect becomes particularly relevant in the next section, where lower proton energies are investigated in more detail. For energies above ~10 MeV, the protons have sufficient energy to fully traverse the fiber while the Bragg peak lies outside the fiber.

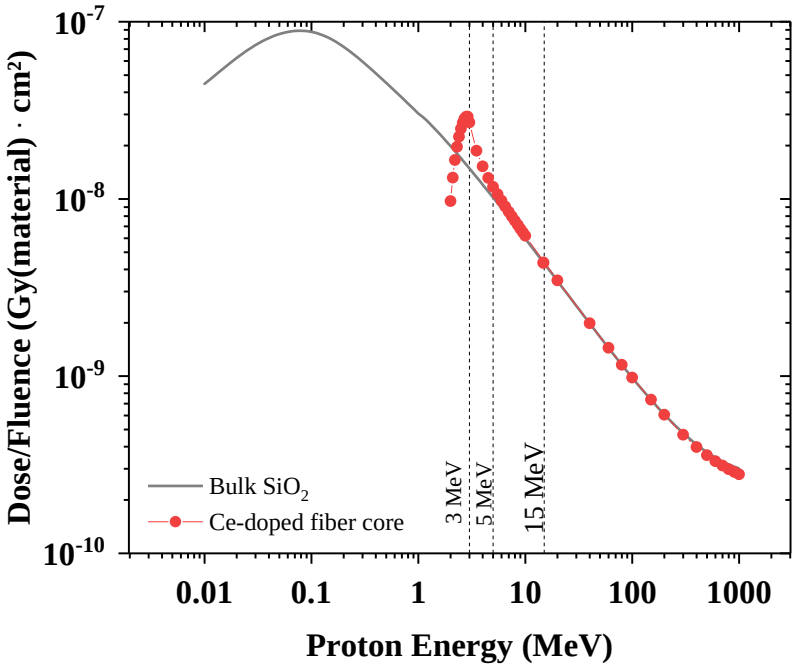

Figure 5: Geant4 simulations of Dose/Fluence vs the proton beam energy on Ce^{3+}-doped optical fiber. Results are compared with bulk silica from SRIM data. Dashed lines indicate the proton energies used in this work. Error bars are smaller than the data point size.

By using the previous calibration done with X-rays in Saint-Etienne for the pre-irradiated optical fiber, it is possible to convert the RIL signal in dose rate and, by dividing this value for the dose/fluence coefficient corresponding to 15 MeV protons, it is possible to estimate the calculated proton flux. These 'calculated' values (with 13% error bars, accordingly to the reproducibility uncertainty) are plotted, in **Figure 6,** against the 'nominal' flux values ($\pm$ 10%) provided by the facility.

The correlation displays a linear trend with a data spread of approximately 24%. This dispersion can be considered as the current uncertainty margin of the proposed dosimetry method, which can be certainly improved through additional tests where the calibration (done with 10% precision with our X-ray machine) can be more accurately validated.

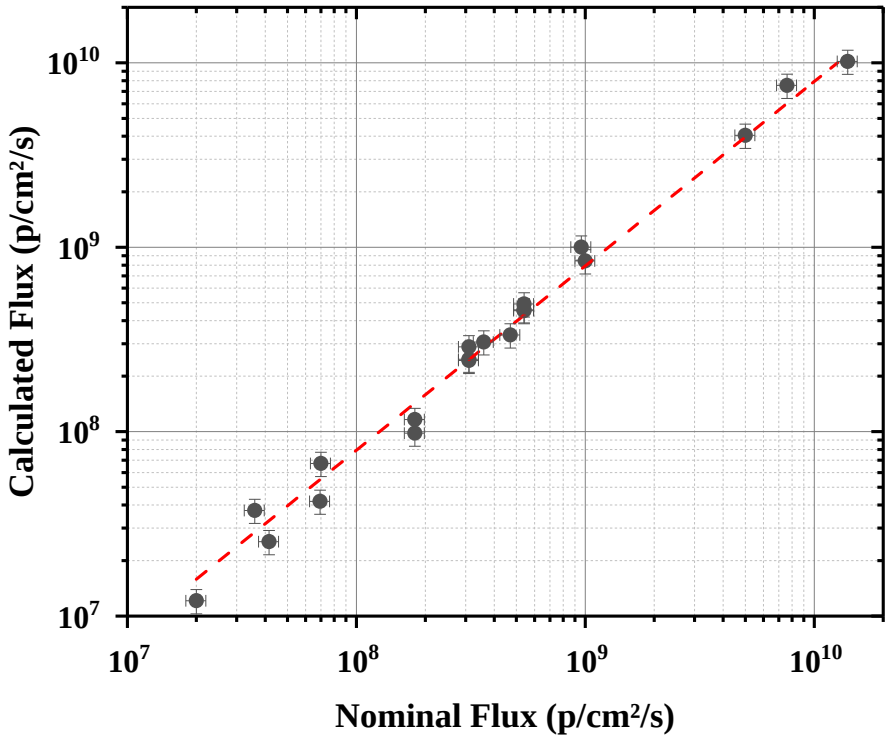

Figure 6: 15 MeV energy proton flux calculated starting from the RIL signal of the pre-irradiated fiber; the Geant4 coefficient allow to convert dose into proton fluence and the pre-calibration under X-rays let obtain the number of counts in dose, as a function of the nominal flux provided by the CNA facility.

3.2. 3-5 MeV protons

Using the Tandem facility, with the proton beam traveling in vacuum, it was possible to test the response of the fibers at even lower energies, specifically at 3 and 5 MeV. For this second part of the study, only the pre-irradiated fiber was selected since previous measurements had shown its more sensitive radiation response.

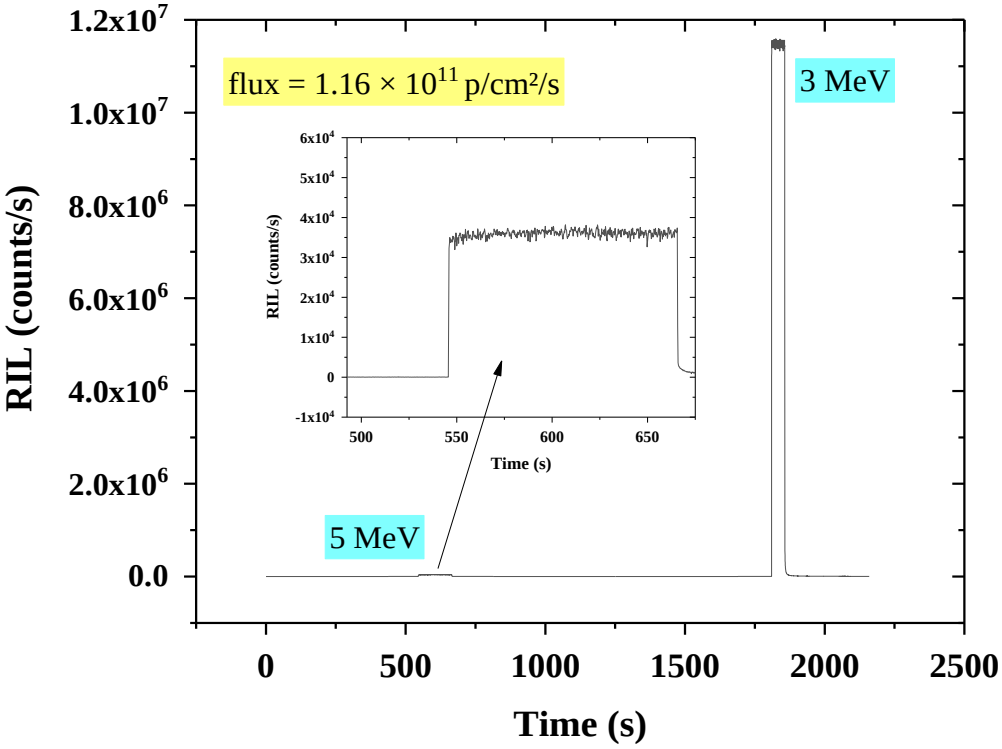

Figure 7: RIL kinetics for the pre-irradiated fiber, acquired under the same flux but with protons of different energies. The inset is a zoom of the recorded signal by exposing the fiber to 5 MeV protons.

In **Figure 7**, we report the most representative result of the acquired data. It is interesting to note from the illustrated kinetics that two distinct radioluminescence levels were recorded on the same fiber under the same proton flux, by varying only the beam energy. The first run, shown in the inset with a zoom, was acquired under 5 MeV protons exposure. Maintaining the same flux but lowering the energy to 3 MeV results in much higher radioluminescence level, as observed during the second run. These results are likely due to the different deposited doses per unit of fluence, as previously discussed for **Figure 5**. As further confirmation of this aspect, **Figure 8** shows the result of a Geant4 simulation of the dose-to-fluence ratio for three different proton energies passing through a 1.5 cm × 1.5 cm square bulk silica. Under the Continuous Slowing Down Approximation (CSDA), the electronic stopping power of protons (proton–electron interactions being the dominant contribution) can be considered equivalent to the Linear Energy Transfer (LET). Therefore, the dose-to-fluence ratio is proportional to the LET per unit material density. The simulation thus provides an idea of the LET for the considered energies. Considering the fiber dimensions, we observe that at 5 MeV the Bragg Peak lies

beyond the fiber limits, and for 15 MeV protons it is even beyond the bulk silica. For 3 MeV protons, however, the Bragg Peak is expected to be located at the core–cladding interface, leading to a non-uniform energy loss within the fiber core.

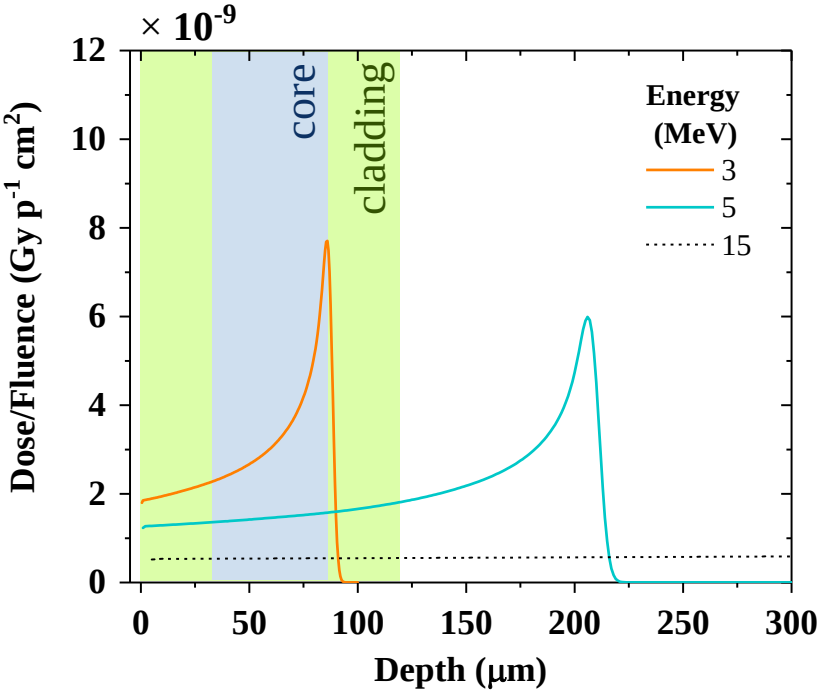

Figure 8: Simulated dose/fluence of different energy protons in a bulk silica. The colored boxes correspond highlight the core and cladding fiber dimensions.

However, experimentally, one would expect to observe the same ratio of the RIL signal as the dose/fluence values for the simulated fiber geometry from **Figure 5** at 3 and 5 MeV energy, being 2.2. Instead, from the kinetics in **Figure 7**, the ratio between the two radioluminescence levels is ~126.

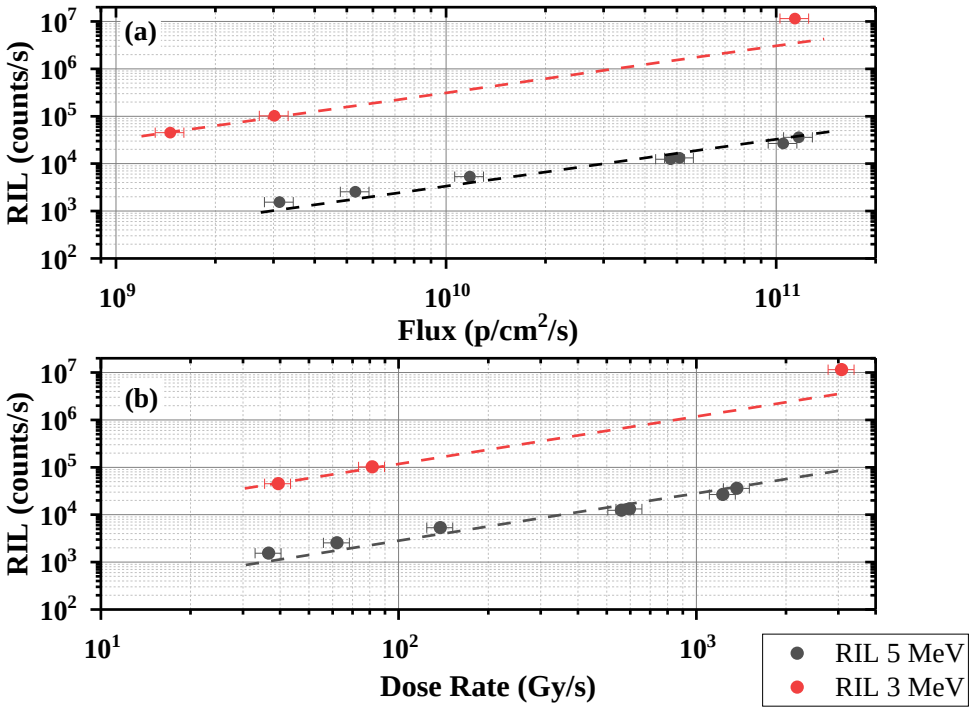

Figure 9: RIL as a function of (a) the nominal flux and (b) the estimated equivalent dose rate, using protons of 3 MeV (red data) and of 5 MeV (black data).

Figure 9(a) illustrates the RIL values from other runs as a function of the facility nominal flux, for the two energies. Thus, in this case, changing the energy necessarily requires the use of a different calibration. The earlier observation in a precedent work [13] that the same calibration could be used within the 23 to 63 MeV range seems not valid in this case. This discrepancy arises because the Bragg peak occurs within the fiber, and therefore the deposited dose differs depending on the proton energies. Specifically, although the Bragg peak is inside the fiber at both energies, at 5 MeV it is probably more localized in the cladding, whereas at 3 MeV it lies inside the core or at its interface. According to the simulation shown in **Figure 5**, the Bragg peak is expected to occur exactly within the core around 2 MeV.

Taking into account the dose/fluence factors for 3 and 5 MeV, an equivalent dose rate is obtained by multiplying these values by the nominal fluxes provided by the facility. The resulting graph is given in **Figure 9(b)** showing the RIL signal as a function of the estimated dose rate for both proton energies. Ideally, the data points should align on the same line since the deposited dose quantities are accounted for. But, as already observed, the ratio of RIL levels is still higher than the dose/fluence ratio at the two energies. Moreover, linearity is lost at high dose rates for 3 MeV protons.

As a preliminary observation, additional measurements are clearly necessary to gather more data and better characterize the linear dependence. It is also important to note that the here-estimated equivalent dose rates are very high and fall within a range never tested before with these fibers. According to [12], non-linearity problems arise starting at around 30 Gy/s for cerium-doped silica glass. This phenomenon is likely linked to radiation-assisted recombination of carriers from transient traps, which produces an extra signal. Although this hypothesis has not been confirmed yet, it suggests the possible involvement of additional physical processes. In particular, those low energy protons can produce significant amount of displacement damages. Even if, for now, the contribution of displacement damages remains limited in the responses of optical fibers, the influence of those processes on the RIL should be investigated in more details for this application.

Also, these are preliminary tests with limited statistical significance. Nevertheless, the results merit further investigation and extension, as miniaturized geometries such as optical fibers could allow for even better monitoring of low-energy protons compared to high-energy ones, due to the higher dose deposition and consequently enhanced radioluminescence intensity, leading to improved sensitivities.

In a future campaign, for example, it could be possible to consider testing the same fiber at each achievable energy step in the range from 1 to 5 MeV (e.g., in 0.5 MeV increments) to effectively observe any trend in radioluminescence increase and verify if the dose deposition can be reconstructed in agreement with Geant4 simulations.

4. Conclusions

We introduced the concept of using optical fibers to measure low-energy proton flux, offering a potential real-time dosimetry solution at the CNA research center. Two separate facilities allowed testing of pristine and pre-irradiated optical fibers under monoenergetic protons at 15 MeV, as well as protons with energies ranging from 3 to 5 MeV. This is quite a new topic, since these fibers have never been tested under such low proton energies. We demonstrate that the fiber is extremely sensitive to low-energy protons and, consequently, fibers are perfectly suitable for monitoring the low flux of this beam, a task that has been challenging for the CNA facility.

The small geometry of the fiber allows the proton Bragg peak to occur within the fiber itself. When this happens, our preliminary results suggest that the sensor sensitivity becomes highly energy-dependent, making it impossible to use the same calibration (at a first step) for different energies, as it was observed in other measurement campaigns at higher proton energies.

In this context, it will be essential to verify how the geometry may influence the dose deposition as a function of proton energy, since the same flux at different energies can produce different levels of radioluminescence. The employment of different fiber geometries could help in proton energy discrimination. Additional measurements are certainly needed to investigate the calibration in this energy range and to understand which physical phenomena might be involved in the radioluminescence increase.

Received: ((will be filled in by the editorial staff))
Revised: ((will be filled in by the editorial staff))
Published online: ((will be filled in by the editorial staff))

References

1. J. V. Logan, M. P. Short, P. T. Webster, C. P. Morath, and E. H. Steenbergen, 'Impact of proton-induced transmutation doping in semiconductors for space applications', *Journal of Materials Chemistry C*, vol. 7, no. 29, pp. 8905–8914, 2019.
2. J. L. Barth, K. A. LaBel, and C. Poivey, 'Radiation assurance for the space environment', in *2004 International Conference on Integrated Circuit Design and Technology (IEEE Cat. No.04EX866)*, (Austin, TX, USA: IEEE, 2004): 323–333. doi: 10.1109/ICICDT.2004.1309976.
3. A. Brown and H. Suit, 'The centenary of the discovery of the Bragg peak', *Radiotherapy and Oncology*, vol. 73, no. 3, pp. 265–268, Dec. 2004, doi: 10.1016/j.radonc.2004.09.008.
4. S. Girard et al., 'Recent advances in radiation-hardened fiber-based technologies for space applications', *Journal Optics*, vol. 20, no. 9, (2018):093001, doi: 10.1088/2040-8986/aad271.
5. A. Darafsheh, R. Taleei, A. Kassaee, and J. C. Finlay, 'Proton therapy dosimetry using the scintillation of the silica fibers', *Optics Letters*, vol. 42, no. 4, (2017):847, doi: 10.1364/OL.42.000847.
6. S. Girard et al., 'Overview of Radiation Effects on Silica-Based Optical Fibers and Fiber Sensors', *IEEE Transaction on Nuclear Science*, vol. 72, no. 4, pp. 982-1020, April 2025, doi: 10.1109/TNS.2024.3511455.
7. F. Moretti, G. Patton, A. Belsky, A. G. Petrosyan, and C. Dujardin, 'Deep traps can reduce memory effects of shallower ones in scintillators', *Physical Chemistry Chemical Physics*, vol. 18, no. 2, pp. 1178–1184, 2016, doi: 10.1039/C5CP05711F.
8. M. J. Marrone, 'Radiation-induced luminescence in silica core optical fibers', *Applied Physics Letters*, vol. 38, no. 3, pp. 115–117, Feb. 1981, doi: 10.1063/1.92294.
9. A. Meyer et al., 'X-Ray Radioluminescence in Diversely Doped Multimode Silica-based Optical Fibers', *IEEE Transaction on Nuclear Science*, vol. 69, no. 7, pp. 1625-1632, July 2022, doi: 10.1109/TNS.2022.3140392.
10. M. Cieslikiewicz-Bouet et al., 'Investigation of the Incorporation of Cerium Ions in MCVD-Silica Glass Preforms for Remote Optical Fiber Radiation Dosimetry', *Sensors*, vol. 21, no. 10, (2021):3362, doi: 10.3390/s21103362.
11. I. Zghari *et al.*, 'Radioluminescence Processes in Cerium-Doped Silica Glasses', *IEEE Transaction on Nuclear Science*, vol. 70, no. 8, pp. 1933–1941, Aug. 2023, doi: 10.1109/TNS.2023.3244218.

12. H. El Hamzaoui et al., ‘Cerium-activated sol–gel silica glasses for radiation dosimetry in harsh environment’, *Materials Research Express*, vol. 3, no. 4, Apr. 2016, doi: 10.1088/2053-1591/3/4/046201.
13. F. Fricano *et al.*, ‘Very High Dose Rate Proton Dosimetry With Radioluminescent Silica-Based Optical Fibers’, *IEEE Transactions on Nuclear Science*, vol. 71, no. 8, pp. 1829–1836, 2024, doi: 10.1109/TNS.2024.3378803.
14. N. Savard, D. Potkins, J. Beaudry, A. Jirasek, C. Duzenli, and C. Hoehr, ‘Characteristics of a Ce-Doped silica fiber irradiated by 74 MeV protons’, *Radiation Measurements*, vol. 114, pp. 19–24, Jul. 2018, doi: 10.1016/j.radmeas.2018.03.010.
15. L. Weninger et al., ‘Potential of radioluminescent silica-based optical fibers for 14 MeV neutron beam monitoring’, *Results in Optics*, vol. 19, (2025):100807, doi: 10.1016/j.rio.2025.100807.
16. D. Söderström et al., ‘Radioluminescence Response of Ce-, Cu-, and Gd-Doped Silica Glasses for Dosimetry of Pulsed Electron Beams’, *Sensors*, vol. 21, no. 22, (2021):7523, doi: 10.3390/s21227523.
17. E. Mones et al., ‘Ce-doped optical fibre as radioluminescent dosimeter in radiotherapy’, *Radiation Measurements*, vol. 43, no. 2, pp. 888–892, Feb. 2008.
18. N. Kerboub, ‘Fiber-based dosimetry applied to space research and high energy physics facilities’, PhD’s dissertation, Université Jean-Monnet (departement Optique et Photonique), Saint-Etienne (departement Optique et Photonique), 2023.
19. F. Fricano *et al.*, ‘Preirradiation Treatment Influence on the Radioluminescence of a Nitrogen-Doped Optical Fiber Dosimeter’, *Physica Status Solidi (a)*, vol. 221, no. 3(2024): 2300665.
20. M. A. Respaldiza et al., ‘Accelerator-based research activities at “Centro Nacional de Aceleradores”, Seville (Spain)’, *Nuclear Instruments and Methods in Physics Research Section B: Beam Interactions with Materials and Atoms*, vol. 266, no. 10, pp. 2105–2109, May 2008, doi: 10.1016/j.nimb.2008.02.080.
21. Y. Morilla et al., ‘Progress of CNA to become the Spanish facility for combined irradiation testing in aerospace‘, 2018 18th European Conference on Radiation and Its Effects on Components and Systems (RADECS), Goteborg, Sweden, 2018, doi: 10.1109/RADECS45761.2018.9328656.
22. J. F. Ziegler, M. D. Ziegler, and J. P. Biersack, ‘SRIM – The stopping and range of ions in matter (2010)’, *Nuclear Instruments and Methods in Physics Research Section B: Beam Interactions with Materials and Atoms*, vol. 268, no. 11–12, pp. 1818–1823, Jun. 2010, doi: 10.1016/j.nimb.2010.02.091.
23. F. M. Khan and J. P. Gibbons, ‘Khan’s the physics of radiation therapy, Lippincott Williams & Wilkins, 2014.
24. A. Darafsheh, R. Taleei, A. Kassaee, and J. C. Finlay, ‘The visible signal responsible for proton therapy dosimetry using bare optical fibers is not Čerenkov radiation: Čerenkov radiation is not responsible for proton dosimetry’, *Medical Physics*, vol. 43, no. 11, pp. 5973–5980, Oct. 2016, doi: 10.1118/1.4964453.
25. S. Agostinelli et al., ‘Geant4—a simulation toolkit’, *Nuclear Instruments and Methods in Physics Research Section A: Accelerators, Spectrometers, Detectors and Associated Equipment*, vol. 506, no. 3, pp. 250–303, Jul. 2003, doi: 10.1016/S0168-9002(03)01368-8.
26. J. Allison *et al.*, ‘Recent developments in Geant4’, *Nuclear Instruments and Methods in Physics Research Section A: Accelerators, Spectrometers, Detectors and Associated Equipment*, vol. 835, pp. 186–225, Nov. 2016, doi: 10.1016/j.nima.2016.06.125.